Three-Coordinate Copper(II)−Phenolate Complexes

Brian A. Jazdzewski, Patrick L. Holland, Maren Pink, Victor G. Young, Jr., Douglas J. E. Spencer, and William B. Tolman*

Department of Chemistry and Center for Metals in Biocatalysis, University of Minnesota, 207 Pleasant Street SE, Minneapolis, Minnesota 55455

Received June 11, 2001

The reactions of LCuCl (L = 2,4-bis((2,6-diisopropylphenyl)imido)pentane (L^{iPr}), 2,4-bis((2,6-diisopropylphenyl)-imido)-3-chloropentane (L^{CliPr})) with the phenolates TlOAr (Ar = $C_6H_3Me_2$, C_6H_4OMe, C_6H_4tBu) and $NaOC_6H_3(tBu)_2$ were explored. Novel three-coordinate Cu(II)−phenolates, LCuOAr, were isolated from the reactions with the thallium phenolates and were characterized by X-ray crystallography and spectroscopy (UV−vis, EPR). The complexes feature short Cu−O(phenolate) distances (average Cu−O = 1.81 Å) and, with one exception, irregular N−Cu−O(phenolate) angles that differ within each compound ($15° < \Delta < 28°$, where $\Delta = \angle N_1-Cu-O - \angle N_2-Cu-O$). The exception is $L^{iPr}Cu(OC_6H_4tBu)$, for which X-ray structures at −100 and 25 °C differed due to an unusual reversible phase change with nonmerohedral twinning (2:1 ratio) in the low-temperature form. The high-temperature form has local C_{2v} symmetry ($\Delta = 0°$), and upon cooling below the phase transition temperature (−8 ± 5 °C) lateral movement of the phenolate ligand ($\Delta = 17.6°$) and rotation of the phenolate plane by 10.7° occurs. Resonance Raman spectroscopic data acquired for $L^{iPr}Cu(OC_6H_4tBu)$ corroborated assignment of phenolate → Cu(II) LMCT character in the UV−vis spectra. Cyclic voltammetry experiments (THF, 0.5 M NBu_4PF_6) revealed negative $E_{1/2}$ values for the Cu(II)/Cu(I) couples relative to NHE, consistent with enhanced stabilization of the Cu(II) state by both the strongly electron donating β-diketiminate ligand and the phenolates. Although thermally stable, the Cu(II)−phenolates are unusually reactive with dioxygen, albeit to give product(s) that have yet to be identified. In the reaction of $L^{iPr}CuCl$ with $NaOC_6H_3(tBu)_2$ no Cu(II)−phenolate was observed. Instead, a Cu(I) complex was generated quantitatively by trapping with added isocyanide, [$L^{iPr}CuNC(C_6H_3Me_2)$], along with 3,3′,5,5′-tetra-*tert*-butyl-4,4′-dibenzoquinone and 2,6-di-*tert*-butylphenol in 27 ± 3% and 46 ± 6% yields, respectively, corresponding to the overall reaction $4L^{iPr}Cu^{II}Cl + 4NaOAr \rightarrow 4L^{iPr}Cu(I) + 4NaCl +$ dibenzoquinone + 2(phenol).

Introduction

Considerable recent emphasis has been placed on the detailed study of the properties of Cu(II)−phenolate complexes because of their postulated involvement in a range of biological and catalytic processes. Thus, Cu(II)−phenolate units have been proposed as intermediates in the catalytic cycles of metalloenzymes (e.g., galactose oxidase,[1] tyrosinase[2]), in the biogenesis of novel metalloenzyme cofactors (e.g., topaquinone in amine oxidases[3]), and in synthetic catalysis (e.g., alcohol oxidation,[4] phenol polymerization[5]).[6] The known Cu(II)−phenolate complexes exhibit coordination numbers ranging from 4 to 6, as is typical for the coordination chemistry of Cu(II). In addition, the phenolates in most of these compounds usually are incorporated as part of multidentate ligand systems;[6] complexes with simple, exogenous phenolate ligands are less common.[7] Of particular note are the recently reported series of four-coordinate complexes $Tp^{iPr2}Cu(OAr)$ (Ar = C_6H_4-4-F, C_6H_3-2,6-Me_2, C_6H_3-2,6-*t*Bu) that exhibit unusual thermal and air sensitivity attributed to the contribution of Cu(I)−phenoxyl radical resonance forms to their ground-state structures.[8]

We recently discovered[9] the first example of a three-coordinate Cu(II) complex, $L^{iPr}CuCl$ (L^{iPr} = 2,4-bis(2,6-diisopropylphenylimido)pentane),[10] and showed that it may be converted by metathesis reactions to three- and four-coordinate Cu(II)−thiolate complexes that model various type 1 metalloprotein active sites.[9,11,12] Here we report results of further explorations of the chemistry of three-coordinate Cu(II) ions in which we have examined the reactions of phenolates with $L^{iPr}CuCl$ and with a new derivative that contains an electron-withdrawing chlorine substituent, $L^{CliPr}CuCl$ (Scheme 1). Key findings include the isolation and spectroscopic, electrochemical, and X-ray crystallographic characterization of a new class of Cu(II)−phenolate compounds that exhibit three-coordination and

* To whom correspondence should be addressed. Fax: 612-624-7029. E-mail: tolman@chem.umn.edu.

(1) (a) Whittaker, J. W. In *Metalloenzymes Involving Amino Acid Residue and Related Radicals*; Sigel, H., Sigel, A., Eds.; Marcel Dekker: New York, 1994; Vol. 30, pp 315−360. (b) Knowles, P. F.; Ito, N. In *Perspectives in Bio-inorganic Chemistry*; Jai Press: London, 1994; Vol. 2, pp 207−244. (c) Whittaker, J. W.; Whittaker, M. M. *Pure Appl. Chem.* **1998**, *70*, 903−910.

(2) Solomon, E. I.; Sundaram, U. M.; Machonkin, T. E. *Chem. Rev.* **1996**, *96*, 2563−2605.

(3) (a) Dooley, D. M. *J. Biol. Inorg. Chem.* **1999**, *4*, 1−11. (b) Williams, N. K.; Klinman, J. P. *J. Mol. Catal. B: Enzym.* **1999**, *8*, 95−101.

(4) (a) Wang, Y.; DuBois, J. L.; Hedman, B.; Hodgson, K. O.; Stack, T. D. P. *Science* **1998**, *279*, 537−540. (b) Chaudhuri, P.; Hess, M.; Flörke, U.; Wieghardt, K. *Angew. Chem., Int. Ed. Engl.* **1998**, *37*, 2217−2220. (c) Chaudhuri, P.; Hess, M.; Weyhermüller, T.; Wieghardt, K. *Angew. Chem., Int. Ed.* **1999**, *38*, 1095−1098. (d) Chaudhuri, P.; Hess, M.; Müller, J.; Hildenbrand, K.; Bill, E.; Weyhermüller, T.; Wieghardt, K. *J. Am. Chem. Soc.* **1999**, *121*, 9599−9610.

(5) (a) Hay, A. S. *J. Polym. Sci., Part A: Polym. Chem.* **1998**, *36*, 505−517. (b) Higashimura, H.; Kubota, M.; Shiga, A.; Fujisawa, K.; Morooka, Y.; Uyama, H.; Kobayashi, S. *Macromolecules* **2000**, *33*, 1986−1995 and references therein.

(6) Jazdzewski, B. A.; Tolman, W. B. *Coord. Chem. Rev.* **2000**, *200−202*, 633−685.

10.1021/ic010615c CCC: $20.00
Published on Web 10/13/2001

Scheme 1

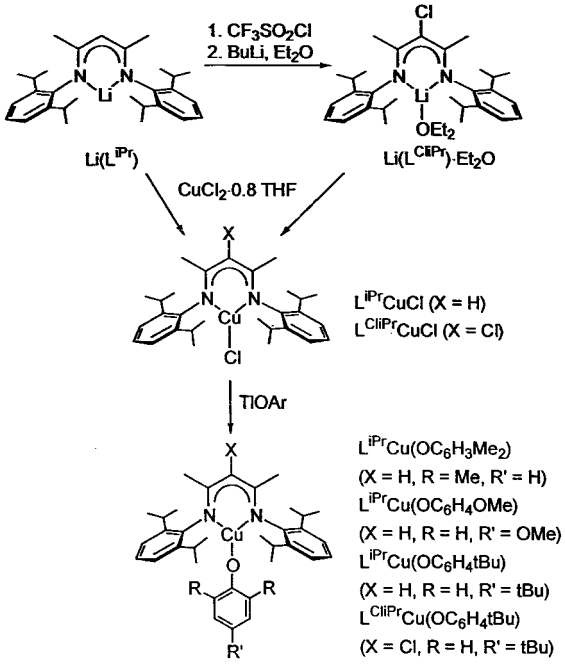

that are thermally stable, yet are dioxygen-sensitive. These results shed new light on the possible nature of intermediates involved in the processing of phenolic species by Cu(II) sites in biology and catalysis.

Results and Discussion

Syntheses. The crystalline ligand Li(L^{CliPr})·Et_2O was prepared by chlorination of the previously reported Li(L^{iPr})[10] with CF_3SO_2Cl followed by deprotonation with *n*BuLi in Et_2O (Scheme 1). The presence of the Et_2O solvate in Li(L^{CliPr})·Et_2O was confirmed by NMR spectroscopy, elemental analysis, and an X-ray crystal structure (see below). Reaction of Li(L^{iPr}) or Li(L^{CliPr})·Et_2O with $CuCl_2$·0.8THF[13] yielded LCuCl (L = L^{iPr}, L^{CliPr}) (Scheme 1). Characterization by X-ray crystallography and spectroscopy (previously described[9] for L = L^{iPr}) confirmed analogous three-coordinate Cu(II) structures for these chloride complexes, which serve as convenient starting materials for the construction of other derivatives via metathesis reactions. Attempts to prepare Cu(II)−phenolate complexes via metathesis of LCuCl (L = L^{iPr}, L^{CliPr}) with sodium salts of several phenolates generally were unsuccessful, however, usually leading to intractable mixtures because of incomplete conversions to products. This problem was obviated by using thallium phenolates TlOAr (Ar = $C_6H_3Me_2$, C_6H_4OMe, C_6H_4tBu) that were prepared by reaction of the phenols HOAr with TlOEt.[14] Treatment of LCuCl with TlOAr resulted in rapid precipitation of TlCl and generation of the series of dark green compounds LCuOAr (Scheme 1), each of which was characterized by spectroscopic, X-ray crystallographic, and analytical methods. The complexes are stable at room temperature under an N_2 atmosphere as solids or in solution for long periods (months). The stability of $L^{iPr}CuOC_6H_3Me_2$ in particular is noteworthy, because the four-coordinate complex of the same phenolate, $Tp^{iPr2}CuOC_6H_3Me_2$, was observed to decay upon warming above −50 °C under Ar to form 3,3′,5,5′-tetramethyldibenzoquinone (albeit in 12% yield).[8]

A different course was followed in the reaction of L^{iPr}CuCl with 1 equiv of sodium 2,6-di-*tert*-butylphenoxide in THF; instead of yielding a dark green solution indicative of copper(II)−phenoxide complex formation, a yellow-brown color developed immediately upon mixing of the reagents. Removal of the solvent under reduced pressure led to product decomposition, as indicated by the formation of a muddy green-brown solution and the deposition of a large amount of insoluble material. The absence of discernible features in the visible region of the optical absorption spectrum of the original reaction mixture led us to suspect that an unstable Cu(I) product was formed by reduction of the Cu(II) starting material (or a species derived therefrom) by the hindered phenoxide. To test this hypothesis, the reaction was repeated, but with 2,6-dimethylphenyl isocyanide added as a Cu(I) trap (Scheme 2). Careful analysis of the reaction by ^{1}H NMR spectroscopy revealed quantitative formation of $L^{iPr}Cu(CNC_6H_3Me_2)$ based on the amount of the starting complex L^{iPr}CuCl. Crystalline $L^{iPr}Cu(CNC_6H_3Me_2)$ was isolated from the reaction mixture in 49% yield and was identified by spectral, analytical, and X-ray diffraction methods. In addition, 3,3′,5,5′-tetra-*tert*-butyl-4,4′-dibenzoquinone and 2,6-di-*tert*-butylphenol were identified by ^{1}H NMR spectroscopy as coproducts in 27 ± 3% and 46 ± 6% yields, respectively, based on the amount of 2,6-di-*tert*-butylphenoxide used. These yields match those expected for the stoichiometry indicated by reaction 1 to within experimental error (25% and 50%).

$$4L^{iPr}Cu^{II}Cl + 4NaOAr \rightarrow 4L^{iPr}Cu^{I} + 4NaCl + \text{dibenzoquinone} + 2(\text{phenol}) \quad (1)$$

The observation of reaction 1 contrasts with the reactivity described previously for the system supported by Tp^{iPr2}.[8] Thus, the complex $Tp^{iPr2}Cu(OC_6H_3tBu_2)$ was reported to be isolable at low temperature and to decay under Ar to yield dibenzo-

(7) A search of the Cambridge Crystallographic Database (v. 5.20, October 2000) revealed the following reports of examples of structurally defined Cu(II) complexes of exogenous phenolates: (a) Bullock, J. I.; Hobson, R. J.; Povey, D. C. *J. Chem. Soc., Dalton Trans.* **1974**, 2037. (b) Wong, R. Y.; Palmer, K. J.; Tomimatsu, Y. *Acta Crystallogr., Sect. B* **1976**, *32*, 567. (c) Yablokov, Y. V.; Simonov, Y. A.; Yampol'skaya, M. A.; Dvorkin, A. A.; Matuzenko, G. S.; Voronkova, V. K.; Mosina, L. V. *Zh. Neorg. Khim.* **1980**, *25*, 2468. (d) Ladd, M. F. C.; Perrins, D. H. G. *Acta Crystallogr., Sect. B* **1980**, *36*, 2260. (e) Yampol'skaya, M. A.; Dvorkin, A. A.; Simonov, Y. A.; Voronkova, V. K.; Mosina, L. V.; Yablokov, Y. V.; Turte, K. I.; Ablov, A. V.; Malinovskii, T. I. *Zh. Neorg. Khim.* **1980**, *25*, 174. (f) Calderazzo, F.; Marchetti, F.; Dell'Amico, G.; Pelizzi, G.; Colligiani, A. *J. Chem. Soc., Dalton Trans.* **1980**, 1419. (g) Dvorkin, A. A.; Matuzenko, G. S.; Simonov, Y. A.; Yampol'skaya, M. A.; Gerbeleu, N. V.; Malinovskii, T. I. *Zh. Neorg. Khim.* **1982**, *27*, 365. (h) Marengo-Rullan, J. R.; Willet, R. D. *Acta Crystallogr., Sect. C* **1986**, *42*, 1487. (i) Kwik, W.-L. *J. Coord. Chem.* **1988**, *19*, 279. (j) Whittaker, M.; Chuang, Y.; Whittaker, J. *J. Am. Chem. Soc.* **1993**, *115*, 10029−10035. (k) Ji, B.; Zhou, Z.; Ding, K.; Li, Y. *Polyhedron* **1998**, *17*, 4327. (l) Gokagac, G.; Tatar, L.; Kisakurek, D.; Ulku, D. *Acta Crystallogr., Sect. B* **1999**, *55*, 1413. (m) Tatar, L.; Gokagac, G. *Acta Crystallogr., Sect. C* **2000**, *56*, 668.
(8) Fujisawa, K.; Iwata, Y.; Kitajima, N.; Higashimura, H.; Kubota, M.; Miyashita, Y.; Yamada, Y.; Okamoto, K.; Moro-oka, Y. *Chem. Lett.* **1999**, 739−740.
(9) Holland, P. L.; Tolman, W. B. *J. Am. Chem. Soc.* **1999**, *121*, 7270−7271.
(10) Feldman, J.; McLain, S. J.; Parthasarathy, A.; Marshall, W. J.; Calabrese, J. C.; Arthur, S. D. *Organometallics* **1997**, *16*, 1514−1516.
(11) Holland, P. L.; Tolman, W. B. *J. Am. Chem. Soc.* **2000**, *122*, 6331−6332.
(12) Randall, D. W.; DeBeer, S.; Holland, P. L.; Hedman, B.; Hodgson, K. O.; Tolman, W. B.; Solomon, E. I. *J. Am. Chem. Soc.* **2000**, *122*, 11632−11648.
(13) So, J.-H.; Boudjouk, P. *Inorg. Chem.* **1990**, *29*, 1592−1593.
(14) After this work was completed but prior to submission of this paper, an alternative preparation of $TlOC_3H_3Me_3$ and its X-ray crystal structure were reported: Zechmann, C. A.; Boyle, T. J.; Pedrotty, D. M.; Alam, T. M.; Lang, D. P.; Scott, B. L. *Inorg. Chem.* **2001**, *40*, 2177−2184.

Scheme 2

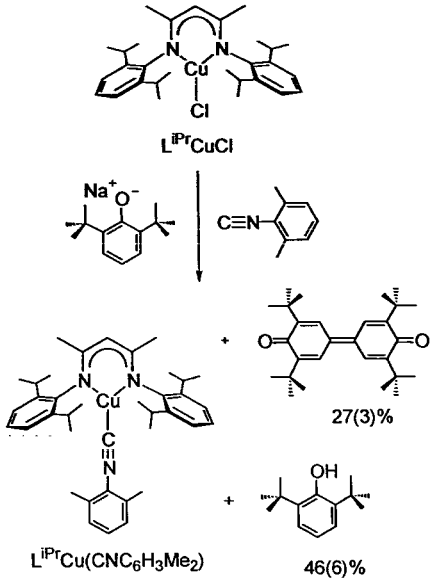

quinone only in 32% yield; no formation of phenol coproduct was cited. While no mechanistic data are available, we speculate that dibenzoquinone formation in both systems involves a similar first step: C−C bond formation between species with phenoxyl radical character (Scheme 3, step 1) as previously suggested[8,15] or, alternatively, between free phenoxyl radicals generated by one-electron reduction of Cu(II) species. Trapping of the Cu(I) coproduct by isocyanide and further oxidation of the dihydrodibenzoquinone would then ensue. In our system the starting $LCu^{II}Cl$ complex or the (unobserved) $LCu^{II}OAr$ species acts as the oxidant (Scheme 3, step 2), yielding the dibenzoquinone and 2 equiv more of Cu(I) species and phenol. This oxidation step must be fast relative to the C−C coupling in order to rationalize the observed yield of phenol coproduct, a rate disparity that may be lessened or reversed in the Tp^{iPr2} system, where no phenol was reported.[8]

X-ray Structures. X-ray crystal structures were solved for $Li(L^{CliPr})\cdot Et_2O$ (Figure 1a), $L^{CliPr}CuCl$ (Figure 1b), each of the phenolate complexes (Figure 1c and Figure S1 in the Supporting Information), and $L^{iPr}Cu(CNC_6H_3Me_2)$ (Figure 1d). Selected crystallographic data and interatomic distances and angles are listed in Tables 1 and 2, respectively. Analysis of the N_2OLi core in $Li(L^{CliPr})\cdot Et_2O$ (Figure 1a) reveals a pattern of divergent bond angles about the Li^+ ion; the β-diketiminate ligand "bite" angle N1−Li1−N2 is 95.04(13)°, while the other two O−Li−N angles are larger (O1−Li1−N1 = 132.27(15)° and O1−Li1−N2 = 132.65(15)°). The lithium ion resides 0.209 Å above the N_2O plane. The structure of $L^{CliPr}CuCl$ (Figure 1b) is closely analogous to that previously reported for $L^{iPr}CuCl$,[9] with both characterized by trigonal-planar, approximately C_{2v} symmetric, three-coordinate geometries and short Cu−N (1.87 ± 0.01 Å) and Cu−Cl (2.13 ± 0.01 Å) distances consistent with their low coordination numbers and Cu(II) oxidation states.

Similar monomeric, three-coordinate formulations were confirmed for each of the Cu(II)−phenolate complexes, with the structure of one, $L^{iPr}Cu(OC_6H_4OMe)$, illustrated in Figure 1c (the others are supplied in Figure S1). Short Cu−O(phenolate) distances are a notable general feature (average Cu−O = 1.81 Å, range 1.79−1.82 Å), with a shorter Cu(II)−O(phenolate) (exogenous) distance having been reported only once previously (1.731(3) Å in $Tp^{iPr2}Cu(OC_6H_4\text{-}4\text{-}F)$).[8] The Cu(II) ions are only slightly displaced from the plane of the ligand N_2O donors (average Cu−N_2O = 0.06 Å, range 0.03−0.10 Å), with the absence of apparent contacts of the metal ion with additional donor atoms being indicative of three-coordination in these compounds. Interestingly, with only one exception, the Cu(II) geometries are irregular, with N−Cu−O(phenolate) angles that differ within each complex so that structures distorted from local C_{2v} symmetry are adopted (15° < Δ < 28°, where Δ = ∠N_1−Cu−O − ∠N_2−Cu−O). This distortion, which is absent in other three-coordinate complexes LCuX (L = L^{iPr}, L^{CliPr}, X = Cl, $SCPh_3$, $SC(Ph)_2CH_2OCH_3$, $SC_6H_3Me_2$),[9,11,12] is accompanied by a translation of the phenolate aryl ring to one side of the axis defined by the Cu−O bond.

Scheme 3

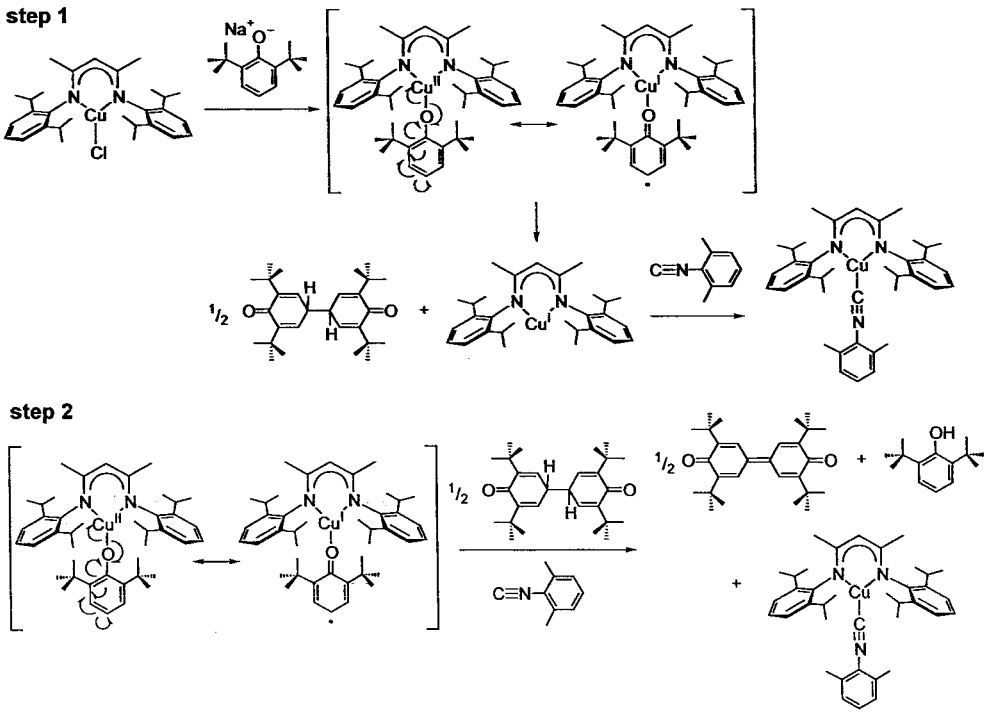

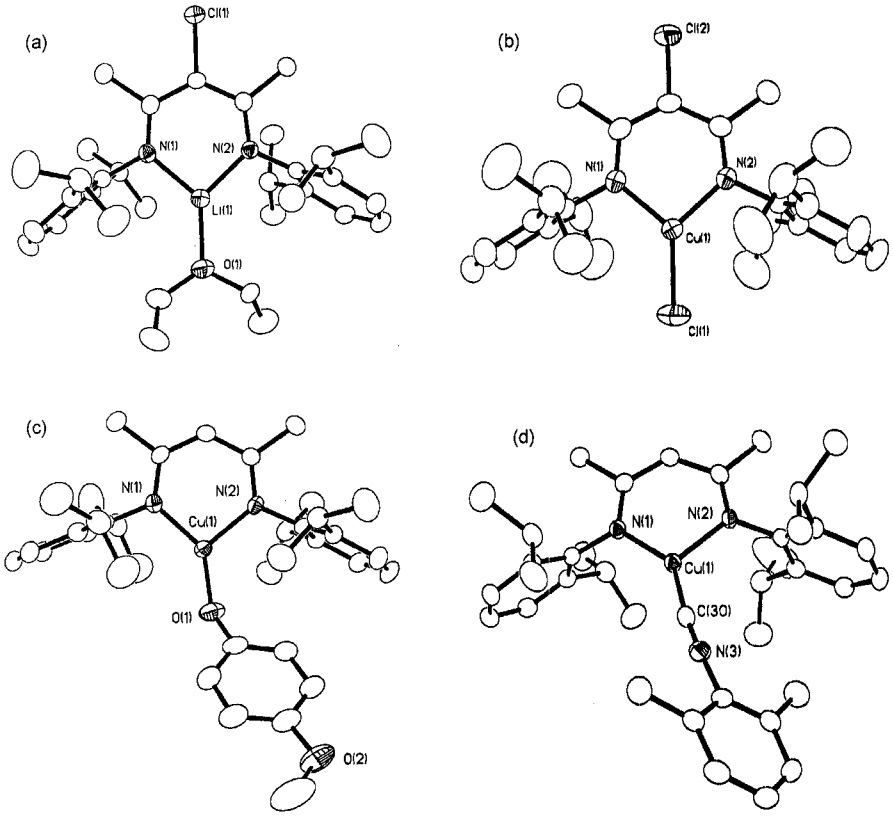

Figure 1. X-ray crystal structure representations of (a) Li(L^{CliPr})·Et_2O, (b) $L^{CliPr}CuCl·CH_2Cl_2$, (c) $L^{iPr}Cu(OC_6H_4OMe)$, and (d) $L^{iPr}Cu(CNC_6H_3Me_2)$. All structures are shown as 50% thermal ellipsoids with only heteroatoms labeled and hydrogen atoms and solvent molecules omitted for clarity.

Table 1. Summary of X-ray Crystallographic Data[a]

	Li(L^{CliPr})·Et_2O	$L^{CliPr}CuCl·CH_2Cl_2$	$L^{iPr}Cu(OC_6H_4OMe)$	$L^{iPr}Cu(OC_6H_3Me_2)$	$L^{iPr}Cu(OC_6H_4tBu)$	$L^{iPr}Cu(OC_6H_4tBu)$[b]	$L^{CliPr}Cu(OC_6H_4tBu)$	$L^{iPr}Cu(CNC_6H_3Me_2)$
empirical formula	$C_{33}H_{50}ClLiN_2O$	$C_{30}H_{42}Cl_4CuN_2$	$C_{36}H_{48}CuN_2O_2$	$C_{37}H_{50}CuN_2O$	$C_{39}H_{54}CuN_2O$	$C_{39}H_{54}CuN_2O$	$C_{39}H_{53}ClCuN_2O$	$C_{38}H_{50}CuN_3$
fwt	533.14	636.00	604.30	602.33	630.38	630.38	664.82	612.35
cryst syst	triclinic	orthorhombic	monoclinic	monoclinic	monoclinic	orthorhombic	monoclinic	triclinic
space group	$P\bar{1}$	*Pbca*	*C*2/*c*	$P2_1/n$	$P2_1/n$	*Pnma*	*C*2/*c*	$P\bar{1}$
a (Å)	11.001(2)	17.189(3)	40.420(2)	9.0263(5)	8.241(1)	21.620(2)	25.6875(18)	8.6687(17)
b (Å)	11.486(2)	18.347(4)	8.4524(5)	20.1213(12)	21.411(2)	20.252(2)	20.0203(13)	12.150(2)
c (Å)	14.182(3)	20.988(4)	19.7553(11)	18.9777(12)	20.185(2)	8.3555(6)	17.5872(11)	17.406(4)
α (deg)	90.25(3)	90	90	90	90	90	90	70.98(3)
β (deg)	98.44(3)	90	99.3350(10)	92.9610(10)	92.920(2)	90	125.0890(10)	79.67(3)
γ (deg)	116.42(3)	90	90	90	90	90	90	82.73(3)
V (Å^3)	1582.7(5)	6619(2)	6660.0(7)	3442.1(4)	3556.9(12)	3658.4(5)	7400.8(8)	1700.5(6)
Z	2	8	8	4	4	4	8	2
d_{calcd} (g cm^{-3})	1.119	1.276	1.205	1.162	1.048	1.145	1.193	1.196
cryst dimens (mm)	0.40 × 0.25 × 0.15	0.35 × 0.25 × 0.25	0.20 × 0.18 × 0.10	0.30 × 0.25 × 0.10	0.18 × 0.18 × 0.15	0.18 × 0.18 × 0.15	0.30 × 0.25 × 0.05	0.40 × 0.30 × 0.20
θ range (deg)	1.46−27.56	1.89−27.49	2.04−27.55	1.48−27.53	1.39−27.50	1.39−27.50	1.40−27.51	1.25−27.49
abs coeff (mm^{-1})	0.147	1.004	0.688	0.663	0.645	0.627	0.693	0.671
no. of rflns collected	16 263	40 235	32 517	21 079	31 489	19 450	22 937	11 970
no. of unique rflns	7077	7583	7608	7835	8156	3343	8430	7319
no. of params	363	344	381	374	402	211	402	383
R1, wR2 ($I > 2\sigma(I)$)[c]	0.0432, 0.1282	0.0436, 0.1029	0.0557, 0.1216	0.0389, 0.0958	0.0598, 0.1415	0.0444, 0.1152	0.0474, 0.0998	0.0409, 0.1036
goodness of fit	0.946	1.026	1.240	0.924	1.048	1.035	0.945	1.037
largest peak, hole (e/Å^3)	0.266, −0.232	0.528, −0.437	0.536, −0.720	0.402, −0.378	0.622, −0.679	0.366, −0.270	0.402, −0.418	0.411, −0.413

[a] All structures determined at $T = -100$ °C, except the indicated structure of $L^{iPr}Cu(OC_6H_4tBu)$. [b] Determined at 25 °C. [c] $R1 = \sum||F_o| - |F_c||/|F_o|$; $wR2 = [\sum w(F_o^2 - F_c^2)^2/\sum w(F_o^2)^2]^{1/2}$, where $w = 1/[\sigma^2(F_o^2 + (aP)^2 + bP]$, $P = (F_o^2 + 2F_c^2)/3$, and *a* and *b* are constants given in the Supporting Information.

Table 2. Selected Bond Distances (Å) and Angles (deg)

	$Li(L^{CliPr})\cdot Et_2O$		
Li1−N1	1.909(3)	Li1−N2	1.913(3)
Li1−O1	1.916(3)		
N1−Li1−O1	132.27(15)	N2−Li1−O1	132.65(13)
N1−Li1−N2	95.04(13)		
	$L^{CliPr}CuCl\cdot CH_2Cl_2$		
Cu1−N1	1.869(2)	Cu1−N2	1.864(2)
Cu1−Cl1	2.1228(8)		
N1−Cu1−Cl1	131.85(7)	N2−Cu1−Cl1	132.00(7)
N1−Cu1−N2	96.09(9)		
	$L^{iPr}Cu(OC_6H_4OMe)$		
Cu1−N1	1.864(2)	Cu1−N2	1.888(2)
Cu1−O1	1.806(2)		
N1−Cu1−O1	140.87(12)	N2−Cu1−O1	122.13(12)
Cu1−O1−C30	128.5(2)	Δ^b	18.74
N1−Cu1−N2	96.66(12)		
	$L^{iPr}Cu(OC_6H_3Me_2)$		
Cu1−N1	1.8825(17)	Cu1−N2	1.8946(17)
Cu1−O1	1.8096(15)		
N1−Cu1−O1	138.76(7)	N2−Cu1−O1	123.98(7)
Cu1−O1−C30	134.94(15)	Δ^b	14.78
N1−Cu1−N2	96.31(8)		
	$L^{iPr}Cu(OC_6H_4tBu)$[c] (−100/25 °C)		
Cu1−N1	1.869(3)/1.880(2)	Cu1−N2/N1A	1.896(3)/
Cu1−O1	1.817(2)/1.794(3)		1.880(2)
N1−Cu1−O1	140.4(1)/131.39(6)	N2/N1A−Cu1	122.8(1)/
Cu1−O1−C30/ C16	117.4(2)/118.1(3)	−O1 Δ^b	131.39(6) 17.60/0
N1−Cu1−N2/NA	96.26(9)/97.10(13)		
	$L^{CliPr}Cu(OC_6H_4tBu)$		
Cu1−N1	1.858(2)	Cu1−N2	1.8959(17)
Cu1−O1	1.8080(17)		
N1−Cu1−O1	145.72(8)	N2−Cu1−O1	117.77(8)
Cu1−O1−C30	123.94(16)	Δ^b	27.95
N1−Cu1−N2	96.26(9)		
	$L^{iPr}Cu(CNC_6H_3Me_2)$		
Cu1−N1	1.9284(17)	Cu1−N2	1.9616(17)
Cu1−C30	1.817(2)		
N1−Cu1−C30	141.76(8)	N2−Cu1−C30	119.96(9)
Cu1−C30−N3	173.64(19)	Δ^d	21.80
N1−Cu1−N2	98.20(7)		

[a] Estimated standard deviations in parentheses. [b] Δ = (N1−Cu1−O1) − (N2/N1A−Cu1−O1). [c] At −100 °C. [d] Δ = (N1−Cu1−C30) − (N2−Cu1−C30).

The exception is $L^{iPr}Cu(OC_6H_4tBu)$, for which X-ray structures determined at 25 and −100 °C differed significantly due to an unusual reversible (nondestructive) phase change accompanied by conversion to a nonmerohedral twin. This phase change is signaled by a change in cell setting (orthorhombic to monoclinic), space group (*Pnma* to $P2_1/n$), and overall structure of the complex upon cooling. Careful analysis of cell parameters obtained for a single crystal examined over a range of temperatures showed that the phase change is fully reversible and occurs at −8 ± 5 °C. The low-temperature phase comprises a nonmerohedral twin (2:1 ratio) that may be visualized by comparing two zone images (a^* based on the high-temperature orthorhombic cell) from X-ray data collections of sample frames showing the same region of reciprocal space at low and high temperatures (Figure S2). Only the major twin component in the low-temperature structure was integrated and solved, with a correction applied for the minor component using ROTWIN.[16]

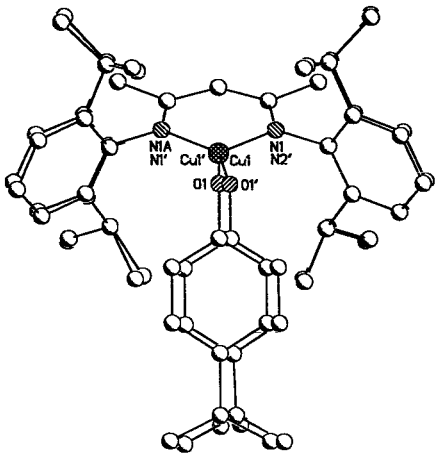

Figure 2. Overlay of the X-ray structures of $L^{iPr}Cu(OC_6H_4tBu)$ determined at 25 and −100 °C, with maximal overlap of the Cu and β-diketiminate backbone N and C atoms to emphasize the differences in the phenolate conformations in the two structures.

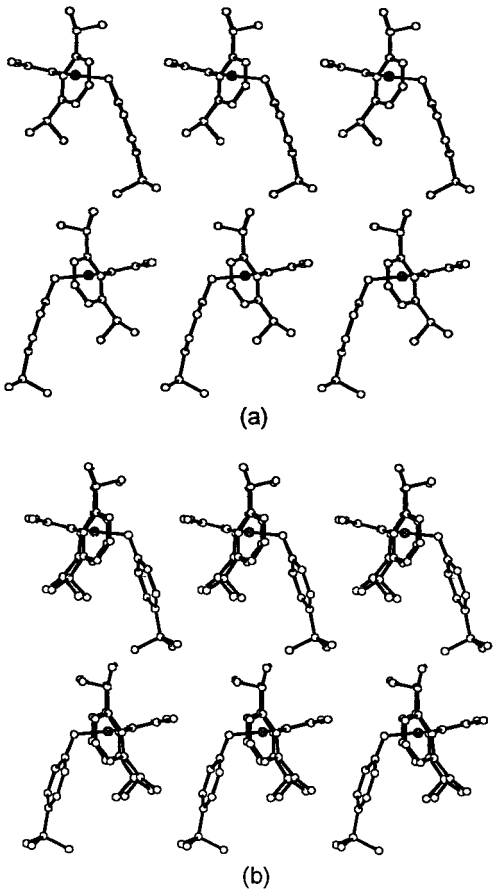

Figure 3. Similarly oriented packing diagrams of the X-ray structures of $L^{iPr}Cu(OC_6H_4tBu)$ determined at (a) 25 °C and (b) −100 °C.

The structures of the complex in the high- and low-temperature phases are compared by an overlay in Figure 2 and by packing diagrams in Figure 3. The low-temperature structure is similar to those of the other phenolate complexes described above, with an asymmetric N_2OCu core characterized by Δ = 17.5°. In contrast, such an angle distortion is absent (Δ = 0°) at high temperature due to the crystallographic mirror plane that bisects the Cu−O(phenolate) bond axis, yielding a C_{2v}-sym-

(15) Kitajima, N.; Koda, T.; Iwata, Y.; Moro-oka, Y. *J. Am. Chem. Soc.* **1990**, *112*, 8833.

(16) Young, V. G., Jr.; Pink, M. ROTWIN: Software for the Creation of HKLF 5 Data from the Twin Law, Metric Tensor, and an Algorithm for Reflection Overlaps; University of Minnesota, 2001 (unpublished).

metric structure. This lateral movement of the phenolate ligand in the phase change is accompanied by a 10.7° shift of the phenolate plane (best seen in Figure 3), a change in the Cu−O bond distance (by 0.03 Å), and small changes in the isopropyl substituents of the β-diketiminate ligand.

The observed retention of crystalline order during the phase change that involves reversible onset of nonmerohedral twinning is unusual, with only a few cases of similar phenomena having been reported previously.[17] Here, the associated geometric changes in the complex suggest an interestingly low thermodynamic preference for a particular direction of the Cu−O(phenolate) bond. In other words, the potential energy surface for lateral movement of the phenolate ligand in the three-coordinate Cu(II) complex appears to be fairly flat. This movement is transmitted over long range in the crystal, resulting in the phase change, with twinning probably resulting because it may occur in either of two directions relative to the mirror plane in the C_{2v}-symmetric form. Perhaps most intriguing is the fact that these relatively large conformational changes in different crystalline domains occur reversibly without any apparent overall damage to the crystal.

Finally, in the X-ray structure of $L^{iPr}Cu(CNC_6H_3Me_2)$ (Figure 1d), the first copper(I) complex of L^{iPr} to be characterized (but see Note Added in Proof), the average Cu−N bond distance of 1.945 Å is longer than even the longest Cu−N distance observed in the copper(II) complexes described above (Cu1−N2 = 1.897(3) Å in the low-temperature structure of $L^{iPr}Cu(OC_6H_4$-tBu)). This expansion is consistent with the lower formal oxidation state for the central metal ion. The coordination geometry is distorted from trigonal planar ($\Delta = 21.80°$), which is not uncommon for Cu(I), and the Cu(I) ion resides slightly above the N_2C plane (by 0.0295(11) Å).

Spectroscopic Properties. The diamagnetic species $Li(L^{CliPr})\cdot Et_2O$ and $L^{iPr}Cu(CNC_6H_3Me_2)$ exhibited sharp ^1H NMR spectra with diastereotopic peaks for the methyl groups on the 2,6-iPr substituents of the aryl rings of the β-diketiminate ligands. These data are consistent with solution structures like those seen in the crystalline state. The Cu(I)−isocyanide complex is colorless, and the optical absorption spectrum has only one feature, an intense band with $\lambda_{max} = 347$ nm ($\epsilon = 28\,300$ $M^{-1}cm^{-1}$). We attribute this band to a β-diketiminate $\pi \rightarrow \pi^*$ transition by analogy to assignments reported previously for some Cu(II) complexes of the same ligand that were based on combined absorption, MCD, and Raman spectroscopic data.[12] In further support of this assignment, a similar band is exhibited by LiL^{iPr} that contains the spectroscopically innocent Li^+ ion.

The X-band EPR spectrum of $L^{CliPr}CuCl$ in 1:1 CH_2Cl_2/toluene (20 K) contains an axial signal with the parameters $g_{||} = 2.20$, $A_{||}(Cu) = 129$ G, $g_\perp = 2.05$, and $A_\perp(N) = 18$ G as determined by spectral simulation (Figure 4a,b). The signal closely resembles that measured previously for $L^{iPr}CuCl$,[9,12] indicating that the Cl substituent on the β-diketiminate backbone does not significantly alter the electronic structure of the complex. Importantly, the large $g_{||}$, small $A_{||}(Cu)$, and large nitrogen superhyperfine $A_\perp(N)$ values distinguish these three-coordinate Cu(II) complexes from more typical tetragonal species and corroborate the previously described high degree of covalency in the bonding between the β-diketiminate ligand and the Cu(II) ion.[12] In further support for the similar electronic

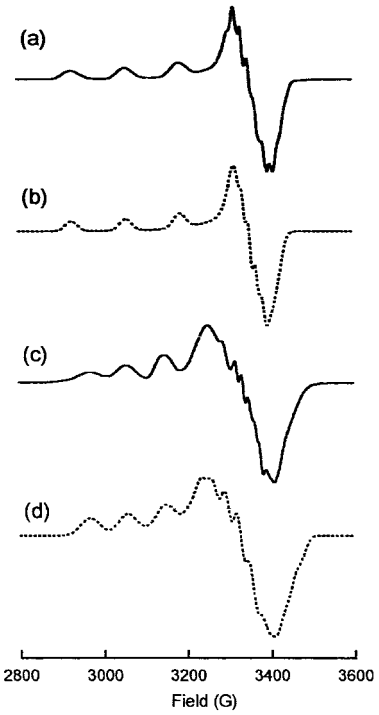

Figure 4. X-band EPR spectra of $L^{CliPr}CuCl$ (a) observed at 20 K in 1:1 CH_2Cl_2/toluene and (b) simulated and of $L^{iPr}Cu(OC_6H_4OMe)$ (c) observed at 20 K in toluene and (d) simulated.

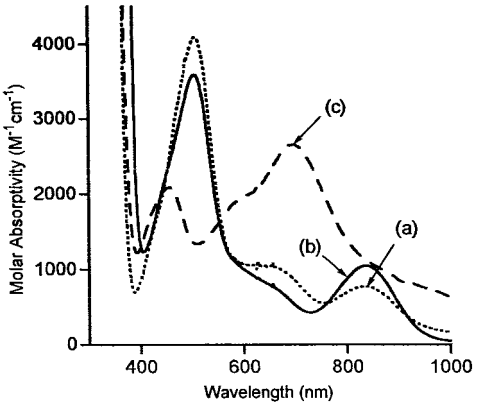

Figure 5. UV−vis absorption spectra of solutions of (a) $L^{iPr}CuCl$ in CH_2Cl_2 (dotted line), (b) $L^{CliPr}CuCl$ in CH_2Cl_2 (solid line), and (c) $L^{iPr}Cu(OC_6H_4tBu)$ in THF (dashed line).

structures of the Cu(II)−chloride complexes supported by L^{iPr} and L^{CliPr}, their electronic absorption spectra are almost identical (Figure 5a,b). Multiple intense absorptions between 400 and 1000 nm are seen that are due to overlapping CT and d−d transitions.[12,18] The absence of any significant shift in these features upon chlorine substitution in the β-diketiminate backbone is a clear sign that the electron-withdrawing effect at the metal ion of such backbone substitution is minor at best.

The copper(II)−phenolate complex $L^{iPr}Cu(OC_6H_4OMe)$ displays an EPR spectrum similar to those of the copper(II)−chloride complexes described above, although adequate simulation required distinct g values (rhombicity) and a reduction in the already low copper-hyperfine splitting value relative to the chloride precursor: $g_z = 2.22$, $A_z = 90$ G, $g_y = 2.07$, $g_x = 2.02$ (Figure 4c,d). In contrast, the spectra observed for the other phenolate complexes are broadened and more complicated (cf.

(17) (a) Colombo, D.; Young, V. G., Jr.; Gladfelter, W. L. *Inorg. Chem.* **2000**, *39*, 4621−4624. (b) Reger, D. L.; Little, C. A.; Young, V. G., Jr.,; Pink, M. *Inorg. Chem.* **2001**, *40*, 2870−2874. (c) Choe, W.; Pecharsky, V. K.; Pecharsky, A. O.; Gschneidner, K. A., Jr.; Young, V. G., Jr.; Miller, G. J. *Phys. Rev. Lett.* **2000**, *84*, 4617−4620.

(18) Randall, D. W.; Holland, P. L.; Tolman, W. B.; Solomon, E. I. Unpublished results.

Figure S3 (Supporting Information) for the spectrum of L^{iPr}-$Cu(OC_6H_4tBu)$ in toluene at 20 K). Variation of solvent (pentane or toluene) and data collection temperature (20 or 77 K) did not perturb the spectra significantly. These data suggest the presence of multiple copper-containing species in the EPR samples, although we note that the complexes used in these experiments were determined to be pure by X-ray crystallographic and analytical methods and integration of the observed signals vs that of an external standard revealed the correct spin quantitation in all cases. One possible rationale for these EPR spectral results would be the existence in solution of phenoxide-bridged dimers of four-coordinate centers, but this appears unlikely on the basis of comparison of the spectral features to those exhibited by other bona fide dimeric complexes of less sterically encumbered β-diketiminates that indicate magnetic coupling interactions.[19] Solvent binding to yield four-coordinate complexes also seems unlikely in view of the poor coordinating abilities of the solvents used, toluene or pentane. Perhaps the most appealing explanation of the EPR data is to invoke the presence of multiple copper(II)−phenolate conformations in solution akin to those seen in the X-ray structures, but further experiments are necessary to confirm this notion (e.g., combined single-crystal EPR/X-ray diffraction analysis).

UV−vis spectra with intense ($\epsilon \approx 1000-3000$ M^{-1} cm^{-1}) absorption features with $\lambda_{max} \approx 450$, 625 (sh), and 700 nm were measured for the dark green β-diketiminate-containing copper(II)−phenolate complexes; a representative spectrum for L^{iPr}-$Cu(OC_6H_4tBu)$ in THF is shown in Figure 5c. On the basis of preliminary resonance Raman experiments (see below) and comparison to other copper(II)−phenolate complexes, we suggest that these absorptions possess at least partial phenolate → copper(II) LMCT character. Additional overlapping contributions from d−d transitions also are likely, by analogy to the results of previous studies of other β-diketiminate−Cu(II) complexes.[12] Comparison of the λ_{max} values for $L^{iPr}Cu(OC_6H_4$-$OMe)$ and $L^{iPr}Cu(OC_6H_4tBu)$, which differ only with respect to the nature of the para phenolate substituent, shows that increasing the electron-donating ability of the phenolate results in a ∼20 nm red shift in the most intense low-energy transition, consistent with predominant phenolate → copper(II) LMCT character for this feature. As was observed in the copper(II)−chloride complexes described above, analysis of the UV−vis spectra for $L^{iPr}Cu(OC_6H_4tBu)$ and $L^{CliPr}Cu(OC_6H_4tBu)$ revealed no significant difference in the observed λ_{max} values, again suggesting that introduction of the Cl substituent in the β-diketiminate backbone does not significantly affect the overall electronic structure of these complexes.

In one instance, $L^{iPr}Cu(OC_6H_4tBu)$, resonance Raman spectral data were obtained in order to lend support to the UV−vis spectral assignments. The Raman spectrum of a CH_2Cl_2 solution measured using 632.8 nm laser excitation is shown in Figure 6. The set of multiple features between 1100 and 1600 cm^{-1} are typical of metal−phenolate complexes and metal−tyrosinate sites in proteins,[20] with those at 1174, 1270, 1500, and 1598 cm^{-1} being diagnostic for coordinated phenolates that have a substituent at the 4-position.[21] On the basis of comparison to previously reported data,[20,21] the bands at 1174 and 1270 cm^{-1} are assigned as C−H bending and C−O stretching modes, respectively, and those at 1500 and 1598 cm^{-1} are attributed to ring C−C stretching vibrations for the coordinated phenolate ligand. Importantly, the strong enhancement of these bands upon excitation at 632.8 nm supports significant contribution of phenolate → copper(II) LMCT to the longest wavelength feature in the absorption spectrum.

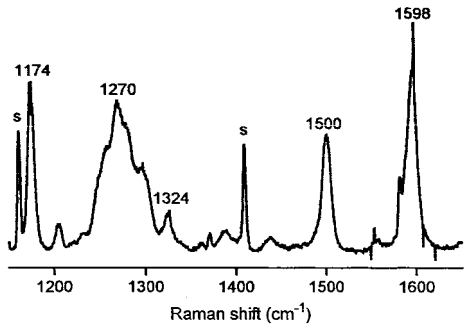

Figure 6. Resonance Raman spectrum of $L^{iPr}Cu(OC_6H_4tBu)$ in CH_2Cl_2 (77 K, $\lambda_{ex} = 632.8$ nm). Peaks marked "s" are derived from the solvent.

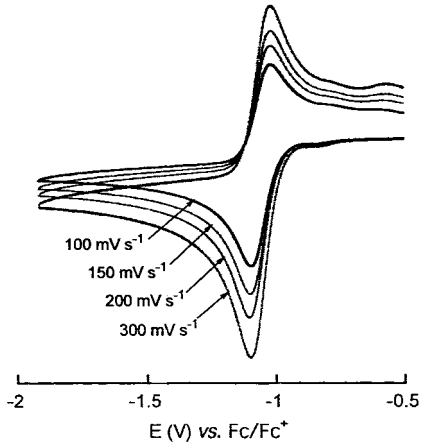

Figure 7. Cyclic voltammograms of $L^{iPr}Cu(OC_6H_4tBu)$ (see text for conditions).

Electrochemistry. Cyclic voltammetry experiments were performed for $L^{iPr}CuOAr$ (OAr = OC_6H_4tBu, OC_6H_4OMe) at room temperature in THF solution with 0.5 M NBu_4PF_6 as supporting electrolyte. Both complexes exhibit a reversible wave when scanned initially to reductive potential, with $i_a \approx i_c$ and an $E_{pa} - E_{pc}$ value of 80 mV that is invariant at scan rates between 100 and 300 mV s^{-1} (Figure 7). We attribute this wave to the Cu(II)/Cu(I) redox couple. When initial scans were taken to oxidative potentials irreversible oxidations were observed at +1.30 V and +1.17 V vs NHE for the complexes with OAr = OC_6H_4tBu, OC_6H_4OMe, respectively, and the Cu(II)/Cu(I) couple became irreversible. We hypothesize that a rearrangement or decomposition reaction occurs upon oxidation at positive potential (perhaps due to phenolate ligand oxidation) and that this is the cause of the loss of reversibility of the Cu(II)/Cu(I) couple. Of particular note is the finding of high potentials for the irreversible oxidation reactions, which appears to belie the air sensitivity of the compounds that is discussed below.

The $E_{1/2}$ values for the Cu(II)/Cu(I) couples of the phenolate complexes are compared in Table 3 to values reported previously (under similar conditions) for other three-coordinate Cu(II) complexes of the same L^{iPr} ligand.[9,11] The negative potentials are consistent with the expected effect of the strongly electron-donating β-diketiminate ligand, which preferentially stabilizes the oxidized metal center.[12] Coordination of a phenolate further destabilizes the Cu(I) form compared to the compounds with

(19) Holland, P. L.; Toia, C.; Jazdzewski, B. A.; Reynolds, A.; Bowen, L.; Tolman, W. B. Unpublished results.
(20) Que, L., Jr. In *Biological Applications of Raman Spectroscopy*; Wiley: New York, 1988; Vol. 3, pp 491−521.
(21) Pyrz, J. W.; Roe, A. L.; Stern, L. J.; Que, L., Jr. *J. Am. Chem. Soc.* **1985**, *107*, 614−620.

Table 3. Values of $E_{1/2}$ for Cu(II) Complexes of L^{iPr} [a]

complex	$E_{1/2}$ (V)	ref
$L^{iPr}CuCl$	−0.08	9
$L^{iPr}CuS(Ph_2)CH_2OMe$	−0.12	11
$L^{iPr}CuSCPh_3$	−0.18	9
$L^{iPr}CuS(Ph_2)CH_2SMe$	−0.20	11
$L^{iPr}CuOC_6H_4tBu$	−0.26	this work
$L^{iPr}CuOC_6H_4OMe$	−0.28	this work

[a] All values reported vs NHE, by adding 800 mV to the value measured vs Fc/Fc^+ in THF with Bu_4NPF_6 as electrolyte (Connelly, N. G.; Geiger, W. E. *Chem. Rev.* **1996**, *96*, 877−910).

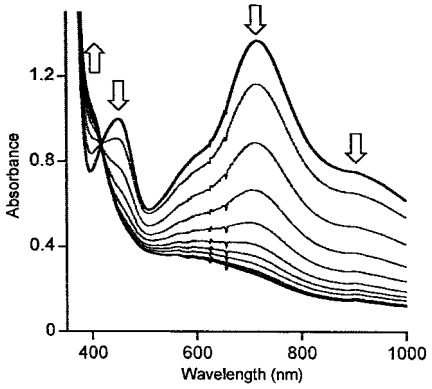

Figure 8. UV−vis absorption spectroscopic changes that occur upon oxygenation of $L^{iPr}Cu(OC_6H_4OMe)$ in THF.

chloride or thiolate ligands, as expected from simple hard/soft acid/base considerations, with a modest additional perturbation caused by the different para substituents (20 mV shift to more negative potential by the more electron-donating OMe group). The redox instability of the Cu(I) form in the entire series of compounds is noteworthy, as one might expect three-coordination to be more favorable for Cu(I) than Cu(II). Instead, ligand charge effects are dominant, and there is little inherent problem with the atypical three-coordinate topology for Cu(II) when supported by the hindered β-diketiminate system.

Dioxygen Reactivity. Unlike most Cu(II)−phenolate complexes, solutions of the compounds LCuOAr are quite air sensitive, as indicated by rapid bleaching of their diagnostic deep green color and associated optical absorption spectral features upon exposure to air or pure O_2. We have not been able to definitively identify the oxygenation product(s), however, despite repeated efforts to characterize the Cu-containing species formed or the organic species remaining after removal of the copper ions. As a case in point, we present results for the oxygenation of $L^{iPr}Cu(OC_6H_4OMe)$; similar data were obtained for $L^{iPr}Cu(OC_6H_4tBu)$.[22] Absorption spectral changes associated with the reaction of $L^{iPr}Cu(OC_6H_4OMe)$ in THF (0.6 mM) with excess O_2 (1 atm, constant bubbling) at 20 °C are shown in Figure 8. The decay of the starting phenolate features follows pseudo-first-order kinetics under these conditions, with $k_{obs} = [1.0(2)] \times 10^{-2}$ s^{-1} ($t_{1/2} = 70$ s). Similar data were obtained at lower temperatures but at slower rates. The light green product solution is EPR silent at 77 K. This product was found to decompose within 24 h at ambient temperature, as indicated by the formation of a light brown solution that lacks the ∼400 nm absorption present in the light green precursor. Attempts to isolate the copper-containing light green intermediate or brown decomposition product have failed to yield discrete copper complexes so far. In an effort to examine the fate of the ligands in the oxygenation/decomposition process, a THF solution of the decomposition product solution was treated with aqueous HCl (6 M) to remove the copper ions and then was extracted with CH_2Cl_2. Analysis of these extracts by GC/MS revealed the presence of 4-methoxyphenol, multiple organic species in small amounts, none of which could be conclusively identified, and $(L^{iPr})H$ that was identified in nearly quantitative yield. These findings indicate that significant β-diketiminate ligand degradation does not occur and that any functionalization of the phenolate occurs to a minor extent to yield a mixture of unidentified products. Although we remain puzzled about the course of the oxygenation reaction, it is clear that the Cu(II)−phenolate unit does react with O_2, thus supporting the notion that such units are competent intermediates in oxidation processes.

(22) Resonance Raman data were acquired for solutions of $L^{iPr}Cu(OC_6H_4tBu)$ that had been treated with $^{16}O_2$ or $^{18}O_2$ (Figure S4, Supporting Information). While new features at 960 and 1557 cm^{-1} were observed, neither shifted upon oxygen isotope substitution.

Summary and Conclusion

By using a straightforward metathesis protocol with selected thallium−phenolates a series of novel three-coordinate Cu(II)−phenolate complexes were prepared and structurally characterized by X-ray crystallography. In one instance, structural differences were observed as a function of temperature due to an unusual reversible phase change accompanied by the onset of nonmerohedral twinning. The formulations of the complexes are corroborated by UV−vis absorption, EPR, and resonance Raman spectroscopic data. Cyclic voltammetry experiments revealed potentials for the Cu(II)/Cu(I) couple that are negative relative to NHE and that are more negative than analogues with chloride or thiolate ligands, consistent with enhanced stabilization of the Cu(II) state by both the strongly electron donating β-diketiminate ligand and the phenolate. Spectral data further show that attachment of a chlorine substituent to the β-diketiminate backbone does not appreciably influence the electronic structure of the Cu(II)−phenolate unit. The Cu(II)−phenolates are unusually air-sensitive, although we have been unable to characterize the oxygenation product(s). Both the low coordination number and the electron-rich nature of the Cu(II) ion in the complexes may be considered as rationales for this reactivity, the finding of which implicates the possible direct involvement of similar Cu(II)−phenolate units in biological and/or catalytic oxidations. Finally, a copper complex of the highly hindered 2,6-di-*tert*-butylphenoxide was not observed; instead, oxidative coupling occurred to yield a Cu(I) complex (trapped with an isocyanide and fully characterized), dibenzoquinone, and phenol (eq 1). While the C−C coupling step of this reaction is similar to that seen in the four-coordinate $Tp^{iPr}CuOAr$ complexes reported previously,[8] the stoichiometry we observe differs, in particular with respect to the yield of phenol, and suggests mechanistic differences between the two systems.

Experimental Section

General Considerations. All solvents and reagents were obtained from commercial sources and used as received unless noted otherwise. The solvents THF, Et_2O, pentane, benzene, and toluene were distilled from Na/benzophenone under nitrogen; CH_2Cl_2 and hexamethyldisiloxane (HMDSO) were distilled from CaH_2 under nitrogen. The concentration of *n*-butyllithium was determined by titration with diphenylacetic acid in THF prior to use. $CuCl_2 \cdot 0.8$THF was prepared according to published procedures.[13] Thallium ethoxide was purchased from Aldrich, filtered through a pad of Celite to remove a small amount of black insoluble material, and stored in the glovebox. Sodium 2,6-di-*tert*-butylphenoxide was prepared by reaction of 2,6-di-*tert*-butylphenol with sodium bis(trimethylsilyl)amide in toluene. 3,3′,5,5′-Tetra-*tert*-butyl-4,4′-benzoquinone was prepared according to a literature

procedure.[23] The complex $L^{iPr}CuCl$ was prepared as described previously.[9] All transition-metal complexes were synthesized and stored in a Vacuum Atmospheres inert-atmosphere glovebox under a dry N_2 atmosphere or by using standard Schlenk and vacuum line techniques.

Physical Methods. NMR spectra were recorded on Varian VI-300, VXR-300, VXR-500, VAC-200, and VAC-300 spectrometers. Chemical shifts (δ) for ^1H and ^{13}C NMR spectra are reported vs tetramethylsilane and referenced to residual protium in the deuterated solvent. IR spectra were recorded on either a Mattson Polaris FTIR or an Avatar 320 FTIR spectrometer. IR samples were prepared as KBr pellets. Routine GC/MS experiments were performed on a Hewlett-Packard 1800A GCD system equipped with a 30 m × 0.25 μm HP-5 column (5% cross-linked PhMe−silicone), 1 mL/min He flow, an initial solvent delay of 2 min at 50 °C, and a ramp rate of 20 °C/min to a final temperature of 250 °C. Quantitation of $(L^{iPr})H$ was accomplished similarly, but with an initial solvent delay of 2 min at 130 °C followed by a ramp rate of 20 °C/min to a final temperature of 250 °C. Elemental analyses were performed by Atlantic Microlabs of Norcross, GA. UV−vis spectra were recorded on a Hewlett-Packard HP8452A (190−820 nm) or HP8453 (190−1100 nm) diode array spectrophotometer. Low-temperature spectra were acquired using a custom-manufactured vacuum Dewar equipped with quartz windows, with low temperatures achieved using a Neslab circulating bath. The cuvette assembly consisted of either a 1 cm or 2 mm quartz cuvet fused to one end of a glass tube while the other end was attached to a high-vacuum stopcock and 14/20 ground glass joint. X-Band EPR spectra were recorded on either a Bruker ESP300 spectrometer fitted with a liquid nitrogen finger Dewar (77 K, approximately 9.44 GHz) or a Bruker E-500 spectrometer, with an Oxford Instruments EPR-10 liquid helium cryostat (20 K, approximately 9.61 GHz). Quantitation of EPR signal intensity for copper complexes was accomplished by comparing the double integration of the derivative spectrum to that of $L^{tBu4}Cu{\cdot}MeOH$[24] or crystalline $L^{iPr}CuCl$[9] in 1:1 CH_2Cl_2/toluene. Where appropriate, EPR spectra were simulated using QPOW.[25] Resonance Raman spectra were collected on an Acton 506 spectrometer using a Princeton Instruments LN/CCD-1100-PB/UVAR detector and ST-1385 controller interfaced with Winspec software. A Spectra-Physics 2030-15 argon ion laser with a power of roughly 40 mW at the sample was employed to give the excitation at 457.9 nm. This argon laser also was used to pump a 375B CW dye (Rhodamine 6G) laser for excitation at 632.8 nm. The spectra were obtained at 77 K using a backscattering geometry; samples were frozen onto a gold-plated copper coldfinger in thermal contact with a Dewar containing liquid nitrogen. Raman shifts were externally referenced to liquid indene. Cyclic voltammetry was performed using Pt working and auxiliary electrodes, a Ag-wire reference electrode, and a BAS Epsilon potentiostat linked to a cell mounted in a Vacuum Atmospheres inert-atmosphere glovebox.

2-((2,6-Diisopropylphenyl)amino)-4-((2,6-diisopropylphenyl)-imino)-3-chloro-2-pentene ($(L^{CliPr})H$). Under a N_2 atmosphere, trifluoromethanesulfonyl chloride (0.70 mL, 6.43 mmol) was added to a cold (−78 °C) solution of $Li(L^{iPr})$[10] (2.60 g, 6.12 mmol) in THF (40 mL), causing bleaching of the solution. The reaction mixture was slowly warmed to ambient temperature with stirring for 1 h. Water (2 mL) and saturated aqueous Na_2CO_3 (15 mL) were then added, causing the deposition of a small amount of white precipitate. An additional 10 mL of H_2O was added, and the solution was extracted with pentane (3 × 75 mL). The organic fractions were combined and dried over $MgSO_4$ and the volatiles removed under reduced pressure to yield a light yellow solid. This solid was dissolved in a minimum amount of warm pentane and slowly cooled to induce the deposition of colorless crystals. Concentration of the supernatant and storage at −20 °C yielded an additional crop (total yield 1.40 g, 50%). ^1H NMR (C_6D_6, 300 MHz): δ 13.21 (br s, 1H), 7.09−7.18 (m, 6H), 3.20 (heptet, J = 6.9 Hz, 4H), 1.95 (s, 6H), 1.12 (dd, J = 6.9 Hz, 24H) ppm. $^{13}C\{^1H\}$ NMR (C_6D_6, 75 MHz): δ 161.6, 143.1, 140.9, 126.6, 124.1, 29.0, 24.7, 23.4, 20.1 ppm; UV−vis (THF; λ_{max}, nm (ϵ, $M^{-1}cm^{-1}$)): 337 (16 500). FTIR (KBr; cm^{-1}): 3063, 2967, 2926, 2867, 1671, 1660, 1605, 1538, 1462, 1437, 1383, 1365, 1325, 1271, 1255, 1239, 1190, 1161, 1102, 1058, 1044, 1017, 1001, 934, 848, 822, 790, 759, 707, 687, 528, 518, 492, 446, 435, 420. LRCIMS: m/z 453.4 ($[M + H]^+$). Anal. Calcd for $C_{29}H_{41}N_2Cl$: C, 76.87; H, 9.12; N, 6.18. Found: C, 77.41; H, 9.35; N, 6.19.

$Li(L^{CliPr}){\cdot}Et_2O$. A solution of $(L^{CliPr})H$ (1.35 g, 2.98 mmol) in Et_2O (20 mL) was cautiously treated with 1.22 mL of *n*-butyllithium (2.56 M in hexanes) at room temperature. After the resulting orange solution was stirred for 30 min, the solvent volume was decreased to 15 mL under reduced pressure and the solution was stored at −20 °C overnight. Colorless crystals deposited, which were washed with cold Et_2O (2 × 2 mL) and dried in vacuo. Further concentration of the supernatant and storage at −20 °C led to the isolation of a second batch (total yield 1.25 g, 79%). ^1H NMR (C_6D_6, 300 MHz): δ 7.01−7.11 (m, 6H), 3.24 (heptet, J = 6.6 Hz, 4H), 2.57 (q, J = 7.2 Hz, 4H), 2.30 (s, 6H), 1.14 (dd, J = 6.6 Hz, 24H), 0.36 (t, J = 7.2 Hz, 6H) ppm. $^{13}C\{^1H\}$ NMR (C_6D_6, 75 MHz): δ 163.6, 149.4, 141.2, 124.0, 123.8, 63.3, 28.5, 24.5, 24.2, 23.4, 13.7 ppm. UV−vis (THF; λ_{max}, nm (ϵ, $M^{-1}cm^{-1}$)): 317 (8800). Anal. Calcd for $C_{33}H_{50}N_2ClLiO$: C, 74.35; H, 9.45; N, 5.25. Found: C, 73.86; H, 9.33; N, 5.40.

$L^{CliPr}CuCl$. To a solution of $Li(L^{CliPr}){\cdot}Et_2O$ (0.400, 0.750 mmol) in THF (25 mL) was added $CuCl_2{\cdot}0.8THF$ (0.144 g, 0.750 mmol) as a solid, causing the development of a dark purple color. The reaction mixture was stirred for 90 min at ambient temperature, and the solvent was removed in vacuo. The purple residue was extracted with CH_2Cl_2 (15 mL) and filtered through a pad of Celite, and the filtrate was evaporated to dryness. HMDSO (10 mL) and CH_2Cl_2 (2 mL) were then added, and the resulting purple solution was stored at −20 °C overnight, yielding purple crystalline material. The volume of the mother liquor was reduced and the solution cooled to give a second crop (total yield 0.217 g, 53%). EPR (1:1 CH_2Cl_2/toluene, 20 K, 9.614 GHz): $g_{\|}$ = 2.20, $A_{\|}(Cu)$ = 129 G, $A_{\|}(N)$ = 3 G, $g_{\perp}$ = 2.05, $A_{\perp}(N)$ = 18 G, $A_{\perp}(Cl)$ = 3 G. UV−vis (CH_2Cl_2; λ_{max}, nm (ϵ, $M^{-1}cm^{-1}$)): 284 (9500), 327 (17 000), 363 (24 500), 505 (3600), 838 (1200). Anal. Calcd for $C_{29}H_{40}N_2CuCl_2$: C, 63.20; H, 7.32; N, 5.08. Found: C, 63.09; H, 7.32; N, 5.07.

General Method for the Preparation of Thallium Phenoxides TlOAr. The appropriate phenol (typically 0.15 g) was dissolved in pentane (5 mL) and the minimum amount of THF (if necessary). The colorless solution was treated with a solution of thallium ethoxide (1 equiv) in pentane (5 mL), causing the immediate precipitation of a colorless solid. The mixture was stirred for 2 h and filtered and the filter cake washed with cold pentane (15 mL). The colorless solid was dried in vacuo to yield pure product in the yields noted.

Thallium 4-Methoxyphenoxide ($Tl[OC_6H_4OMe]$; 96%). ^1H NMR (300 MHz, d_6-DMSO): δ 6.70 (d, J = 8.7 Hz, 2H), 6.60 (d, J = 8.7 Hz, 2H), 3.61 (s, 3H) ppm. $^{13}C\{^1H\}$ NMR (d_6-DMSO, 75 MHz): δ 159.3, 149.4, 117.8, 114.8, 55.5 ppm. Anal. Calcd for C_7H_7OTl: C, 25.67; H, 2.15. Found: C, 25.79; H, 2.11.

Thallium 2,6-Dimethylphenoxide ($Tl[OC_6H_3Me_2]$; 79%). ^1H NMR (300 MHz, d_6-DMSO): δ 6.79 (d, J = 7.2 Hz, 2H), 6.12 (t, J = 7.2 Hz, 1H), 2.38 (s, 6H) ppm. $^{13}C\{^1H\}$ NMR (d_6-DMSO, 75 MHz): δ 164.6, 127.4, 126.2, 112.3, 19.2 ppm. Anal. Calcd for C_8H_9OTl: C, 29.52; H, 2.79. Found: C, 29.85; H, 2.82. For an alternate preparation and a description of the X-ray structure of this compound, see ref 14.

Thallium 4-*tert*-Butylphenoxide ($Tl[OC_6H_4tBu]$; 95%). No NMR data were available, due to lack of solubility. Anal. Calcd for $C_{10}H_{13}OTl$: C, 33.97; H, 3.71. Found: C, 33.92; H, 3.53.

General Method for the Preparation of the Complexes LCuOAr ($L = L^{iPr}, L^{CliPr}$). A solution of LCuCl (typically 0.15 g) in THF (10 mL) was treated with the appropriate thallium phenoxide salt (1.05 equiv) as a solid, causing the development of a dark green color and formation of a white precipitate. After the mixture was stirred for 1 h, the filtrate was evaporated to dryness and the residue redissolved in a minimum amount of pentane. The dark green solution was then filtered through a pad of Celite, and the solvent was removed under reduced

(23) Nishino, H.; Itoh, N.; Magashima, M.; Kurosawa, K. *Bull. Chem. Soc. Jpn.* **1992**, *65*, 620−622.
(24) Halfen, J. A.; Jazdzewski, B. A.; Mahapatra, S.; Berreau, L. M.; Wilkinson, E. C.; Que, L., Jr.; Tolman, W. B. *J. Am. Chem. Soc.* **1997**, *119*, 8217−8227.
(25) (a) Nigles, M. J. Ph.D. Thesis, University of Illinois, Urbana, IL, 1979. (b) Maurice, A. M. Ph.D. Thesis, University of Illinois, Urbana, IL, 1980.

pressure. Recrystallization from pentane at −20 °C gave crystalline solids in the yields noted.

L^{iPr}Cu(OC$_6$H$_4$OMe) (51%). EPR (toluene, 20 K, 9.62 GHz): g_z = 2.22, A_z = 90 G, g_y = 2.07, g_x = 2.02. UV−vis (THF; λ_{max}, nm (ϵ, M^{-1} cm^{-1})): 329 (20 600), 346 (22 400), 450 (2000), 630 (sh, 1800), 717 (2900). Anal. Calcd for $C_{36}H_{48}N_2O_2Cu$: C, 71.55; H, 8.01; N, 4.64. Found: C, 71.43; H, 8.01; N, 4.62.

L^{iPr}Cu(OC$_6$H$_3$Me$_2$) (50%). UV−vis (THF; λ_{max}, nm (ϵ, M^{-1} cm^{-1})): 280 (6500), 344 (21 000), 460 (2100), 643 (sh, 1400), 723 (1800). Anal. Calcd for $C_{37}H_{50}N_2OCu$: C, 73.78; H, 8.37; N, 4.65. Found: C, 73.14; H, 8.29; N, 4.68.

L^{iPr}Cu(OC$_6$H$_4$tBu) (66%). UV−vis (THF; λ_{max}, nm (ϵ, M^{-1} cm^{-1})): 283 (5700), 345 (20 300), 456 (2100), 584 (sh, 1900), 697 (2700). Anal. Calcd for $C_{39}H_{54}N_2OCu$: C, 74.31; H, 8.63; N, 4.44. Found: C, 74.33; H, 8.59; N, 4.45.

L^{CliPr}Cu(OC$_6$H$_4$tBu) (30%). UV−vis (THF; λ_{max}, nm (ϵ, M^{-1} cm^{-1})): 282 (9000), 326 (15 000), 361 (23 500), 458 (1900), 581 (sh, 1800), 699 (2900).

L^{iPr}Cu(CNC$_6$H$_3$Me$_2$). A solution of 2,6-di-*tert*-butylphenol (0.022 g, 0.106 mmol) in THF (2 mL) was treated with NaH (0.009 g, 0.106 mmol) and the mixture stirred under N_2 for 30 min. The reaction mixture was then filtered through a pad of Celite, and the filtrate was treated with a solution of L^{iPr}CuCl (0.050 g, 0.097 mmol) in THF (5 mL). The reaction mixture immediately became light orange. After this mixture was stirred for 0.5 h, a solution of 2,6-dimethylphenyl 1-isocyanide (0.013 g, 0.097 mmol) in THF (1 mL) was added and the reaction mixture was stirred at ambient temperature overnight. The solvent was removed under reduced pressure to yield a orange solid, which was extracted with pentane (20 mL) and filtered through a pad of Celite. The filtrate was then evaporated to dryness, and the residue was dissolved in HMDSO (3 mL) and stored at −20 °C overnight. Pale yellow crystals formed over 3 days (0.029 g, 49%). ^{1}H NMR (C_6D_6, 300 MHz): δ 7.06−7.17 (m, 6H), 6.55 (t, J = 7.5 Hz, 1H), 6.35 (d, J = 7.5 Hz, 2H), 5.03 (s, 1H), 3.57 (heptet, J = 6.9 Hz, 4H), 1.83 (s, 6H), 1.61 (s, 6H), 1.42 (d, J = 6.9 Hz, 12H), 1.26 (d, J = 6.9 Hz, 12H) ppm. ^{13}C{^{1}H} NMR (C_6D_6, 75 MHz): δ 163.8, 150.4, 140.9, 135.4, 128.8, 128.0, 124.3, 123.7, 94.7, 28.6, 25.2, 23.8, 23.7, 18.6 ppm. UV−vis (THF; λ_{max}, nm (ϵ, M^{-1} cm^{-1})): 347 (28 300). FTIR (KBr, cm^{-1}): 3054, 2958, 2922, 2866, 2126 (ν_{CN}), 1545, 1518, 1463, 1439, 1404, 1313, 1254, 1230, 1172, 1102, 1055, 1019, 934, 791, 782, 758, 743, 720, 511, 444. Anal. Calcd for $C_{38}H_{50}N_3Cu$: C, 74.53; H, 8.23; N, 6.86. Found: C, 74.56; H, 8.29; N, 6.94.

NMR Quantification of L^{iPr}Cu(CNC$_6$H$_3$Me$_2$), 2,6-Di-*tert*-butylphenol, and 3,3′,5,5′-Tetra-*tert*-butyl-4,4′-dibenzoquinone. A solution of L^{iPr}CuCl (0.010 g, 0.019 mmol) in THF (2 mL) was treated with 2,6-dimethylphenyl 1-isocyanide (0.0025 g, 0.019 mmol) and a solution of sodium 2,6-di-*tert*-butylphenoxide in THF (2 mL), causing the formation of a light brown solution. The reaction mixture was stirred for 10 min, and the solvent was removed under reduced pressure to yield a light orange solid. This solid was dissolved entirely in 1.0 mL of a 15.3 mM solution of 1,3,5-trimethoxybenzene in C_6D_6, and the sample was analyzed by ^{1}H NMR spectroscopy (delay time 30 s). Chemical shifts for L^{iPr}Cu(CNC$_6$H$_3$Me$_2$), 2,6-di-*tert*-butylphenol, and 3,3′,5,5′-tetra-*tert*-butyl-4,4′-dibenzoquinone were determined from data acquired on independently prepared materials. Integration vs the 1,3,5-trimethoxybenzene standard for selected resonances from each compound was then performed, giving yields of 97 ± 5% for L^{iPr}Cu(CNC$_6$H$_3$Me$_2$), 46 ± 6% for 2,6-di-*tert*-butylphenol, and 27 ± 3% for 3,3′,5,5′-tetra-*tert*-butyl-4,4′-dibenzoquinone.

X-ray Crystallography. Crystal data and collection parameters are listed in Table 1. With one exception (see below), a crystal of the appropriate size was mounted on a glass fiber using hydrocarbon or perfluorinated oil, transferred to a Siemens SMART diffractometer/CCD area detector, and kept at −100 °C. The crystal was then centered in the X-ray beam (Mo Kα radiation; λ = 0.710 73 Å, graphite monochromator) for data collection. Initial cell constants and an orientation matrix were determined by collection of 60 10 s frames, followed by spot integration and least-squares refinement. A minimum of 1.3 hemispheres of data were collected using 0.3° ω scans. The raw data were integrated, and final unit cell constants were calculated using SAINT.[26] Absorption corrections were applied using SADABS[27] unless stated otherwise. The data were corrected for Lorentz and polarization effects, but no correction for crystal decay was applied. Structure solutions were performed with either SHELXS[28] or SIR92.[29] Structure refinements were performed using the programs SHELXTL-Plus V5.0 or SHELXTL V5.1 on a Pentium PC computer. All structure refinements were performed on F^2. Pertinent details for each structure are noted below; see the Supporting Information for full information in the form of CIF files.

Li(L^{CliPr})·Et$_2$O. Crystals suitable for X-ray crystallographic analysis were grown from Et_2O at −20 °C. Partial disorder was found in the coordinated Et_2O molecule. One of the two ethyl arms was rotationally disordered over two positions, with 50% occupancy for each conformation.

L^{CliPr}CuCl·CH$_2$Cl$_2$. Crystals suitable for X-ray crystallographic analysis were grown from a mixture of HMDSO and CH_2Cl_2 (approximately 5:1) at −20 °C. One molecule of CH_2Cl_2 was found in the asymmetric unit. The solvate molecule does not interact with the complex.

L^{iPr}Cu(OC$_6$H$_4$OMe). Crystals suitable for X-ray crystallographic analysis were grown from pentane at −20 °C.

L^{iPr}Cu(OC$_6$H$_3$Me$_2$). Crystals suitable for X-ray crystallographic analysis were grown from HMDSO at −20 °C. Preliminary crystallographic experiments indicated that the compound not only had a phase transition below room temperature but also formed a nonmerohedral twin. The specimen used for final data collection for both phases was glued to a glass fiber with epoxy and transferred to the diffractometer, and an initial data collection was completed at 25 °C without the use of the cryostat. Upon completion of the data collection (1 hemisphere) the cryostat was set at −100 °C and the data collection process was repeated on the same specimen; 1.5 hemispheres of data were collected on the twinned low-temperature polymorph by extending the number of frames collected in each set. Both twin components of the nonmerohedral twin were indexed with GEMINI[30] using reflections gleaned from 3 sets of 30 frames obtained at orthogonal ω settings. The major twin component was indexed with a random set of 73 reflections to cell constants a = 8.263(6) Å, b = 21.429(15) Å, c = 20.187(14) Å, and β = 93.02(2)°. The minor twin component was indexed with 39 of the remaining 41 reflections to the cell constants a = 8.257(8) Å, b = 21.424(19) Å, c = 20.170(18) Å, and β = 92.94(4)°. Reflections that were common to both cells were ignored in the initial determination of cell constants. The twin law (by rows) is [100, 0,−1,0, −0.25,0,−1], which corresponds to 180° rotations about [100] and (100) in reciprocal and direct space, respectively. The difference between the masses of the twin components mandated the integration of only the major twin and applying a correction for the minor twin component with ROTWIN.[16] Of the 8156 total reflections, 2038 had contributions from both twin components. The overall effect was that every $h = 4n$ reflection, where n = −2, −1, 0, 1, 2, had exact overlaps with the other twin component. No partial overlaps were considered when producing the final SHELX HKLF 5 reflection file. A series of a^* zone images on the diffractometer (based on the orthorhombic cell) confirmed that the phase transition occurred at −8 ± 5 °C (see Figure S2 in the Supporting Information).

L^{CliPr}Cu(OC$_6$H$_4$tBu). Crystals suitable for X-ray crystallographic analysis were grown from pentane at −20 °C. Initial attempts to mount the crystals at 25 °C were unsuccessful due to crystal dissolution upon warming of the mother liquor. To avoid this problem, the crystals were mounted at −80 °C. The isopropyl group containing atoms C24−C26 was found to be slightly disordered. Attempts to model this disorder did not lead to significant improvement in the refinement and were not pursued further.

(26) SMART V. 5.1, Software for the Integration of Area Detector Data; Bruker-AXS, Madison, WI.
(27) Blessing, R. H. *Acta Crystallogr.* **1995**, *A51*, 33−38. Sheldrick, G. SADABS V2.03: Program for the Application of Absorption Corrections to Bruker-AXS CCD Single-Crystal Diffraction Data, 2000.
(28) SHELXTL V5.0 and V5.1, Software for the Solution and Refinement of Crystal Structures; Bruker-AXS, Inc.: Madison, WI.
(29) Altomare, A.; Cascarno, G.; Giacovazzo, C.; Gualardi, A. *J. Appl. Crystallogr.* **1993**, 26, 343−350.
(30) GEMINI: Software for Indexing and Correcting Data Affected by Nonmerohedral Twinning; Bruker-AXS, Madison, WI, 1999.

$L^{iPr}Cu(CNC_6H_3Me_2)$. Crystals suitable for X-ray crystallographic analysis were grown from HMDSO at −20 °C.

Acknowledgment. We thank Dr. Raymond Ho and Professor Lawrence Que, Jr., for providing access to the resonance Raman facility, Professor John Lipscomb for access to his EPR spectrometer, Nermeen Aboellela for help with the electrochemical measurements, and the NIH for funding (Grant No. GM47365).

Note Added in Proof. Cu(I) complexes of some β-diketiminate ligands recently have been reported: Yokota, S.; Tachi, Y.; Nishiwaki, N.; Ariga, M.; Itoh, S. *Inorg. Chem.* **2001**, *40*, 5316. Dai, X.; Warren, T. H. *Chem. Commun.* **2001**, 1998.

Supporting Information Available: X-ray crystal structure representations (50% thermal ellipsoids) of $L^{CliPr}Cu(OC_6H_4tBu)$, $L^{iPr}Cu(OC_6H_3Me_2)$, and $L^{iPr}Cu(OC_6H_4tBu)$ at 25 °C and −100 °C (Figure S1), zone images from X-ray data collections of $L^{iPr}Cu(OC_6H_4tBu)$ at 25 and −51 °C surveying identical regions of reciprocal space (Figure S2), an X-band EPR spectrum of $L^{iPr}Cu(OC_6H_4tBu)$ (Figure S3), UV−vis and Raman spectra of oxygenated $L^{iPr}Cu(OC_6H_4tBu)$ (Figure S4), and X-ray crystallographic files, in CIF format, for the structure determinations listed in Table 1. This material is available free of charge via the Internet at http://pubs.acs.org.

IC010615C